The Role of Mineral Aerosol in Tropospheric Chemistry in East Asia—A Model Study

YANG ZHANG* AND GREGORY R. CARMICHAEL

Department of Chemical and Biochemical Engineering, Center for Global and Regional Environmental Research, University of Iowa, Iowa City, Iowa

(Manuscript received 5 February 1998, in final form 18 May 1998)

ABSTRACT

A detailed gas-phase chemistry mechanism is combined with dust surface uptake processes to explore possible impacts of mineral dust on tropospheric chemistry. The formations of sulfate and nitrate on dust are studied along with the dust effects on the photochemical oxidant cycle for the long-range-transported particles with a diameter of 0.1–40 μm.

The results show that mineral dust may influence tropospheric sulfate, nitrate, and O_3 formation by affecting trace gas concentrations and the tropospheric oxidation capacity through surface processes. The postulated heterogeneous mechanism provides a plausible interpretation for the observed high nitrate and sulfate on dust and the anticorrelation between O_3 and dust in East Asia. The presence of dust results in decreases in the concentrations of SO_2 (10%–53%), NO_y^p (16%–100%, defined as $NO_3 + N_2O_5 + HNO_3$), H_xO_y (11%–59%, defined as $OH + HO_2 + H_2O_2$), and O_3 (11%–40%) under model conditions representative of spring dust storms in East Asia. The decrease in solar actinic flux and the surface uptake of O_3 and its precursors contribute to the total O_3 decrease for the conditions studied. Nitrate and sulfate, 0.9–2.1 and 0.3–10 μg m^{-3}, respectively, are formed on dust particles, mostly in the size range of 1.5–10 μm. The magnitude of the dust effect strongly depends on the preexisting dust surfaces, the initial conditions, and the selection of model parameters associated with surface uptake processes. The impact of dust reactions on O_3 reduction is highly sensitive to the uptake coefficient and to the possible renoxification from the surface reaction of HNO_3 on dust.

1. Introduction

Mineral aerosol is an important component in the earth–atmosphere system. Every year 200–5000 metric tons of mineral aerosol are emitted from arid and semiarid regions into the atmosphere (Goudie 1983; Pye 1987). The size of arid regions is increasing by millions of hectares per year due to changes in precipitation and anthropogenic disturbance, including overgrazing, devegetation, erosion, land salinization, and mining activities (Sheehy 1992). The preexisting deserts and the ongoing large-scale desertification have caused the constant seasonal cycle of severe dust storms over many regions including the North Pacific, the mid-Atlantic, the Mediterranean, East Asia, Europe, Africa, and South America (Schütz and Jaenicke 1974; Prospero et al. 1981; Nishikawa et al. 1991a).

While the source, emission, and mass loading of mineral dust on the regional and global scales are now being documented, many effects of dust still remain uncertain. For example, we do not have a good estimate of its radiative effects. Tegen and Fung (1994) have indicated that the uncertainties in calculating the dust optical thicknesses could be a factor of 3–5 because of the crude size resolution, insufficient data, and exclusion of many dynamic processes. We also know little about the surface properties of dust, which largely depend on its microstructure, size and chemical composition, and the ambient conditions. Whether and when the soluble solid substances on a single particle will deliquesce must be determined to fully describe the surface uptake, adsorption/absorption, and chemical reaction processes. Furthermore, the chemical impacts of dust on the trace gas species need to be quantified. Elevated sulfate, nitrate, ozone, and trace metals during dust storms have been recently observed over the Pacific and the Atlantic Oceans (Prospero and Savoie 1989; Savoie and Prospero 1989; NIES 1989; Savoie et al. 1989; Oltmans and Levy II 1992). There remains a question as to what extent the mineral dust behaves as a long-distance carrier and an effective surface interacting with gas-phase species.

We have begun to explore the importance of the dust interactions on tropospheric chemistry. In Dentener et al. (1996), we investigated the impact of irreversible reactions of HNO_3, N_2O_5, NO_3, HO_2, O_3, and SO_2 on dust surfaces on the global scale using a highly parameterized description of gas–aerosol interactions. Results

* Current affiliation: Atmospheric and Environmental Research, Inc., San Ramon, California 94583.

Corresponding author address: Dr. Yang Zhang, AER, Inc., 2682 Bishop Drive, Suite 120, San Ramon, CA 94583.
E-mail: yzhang@aer.com

from that study suggest that a large fraction of gas-phase nitric acid may be neutralized by mineral aerosol. The regions where at least 40% of the total nitrate is found on the mineral aerosol were found to cover vast regions of the Northern and Southern Hemispheres. Only the regions of western and central Europe, the eastern parts of North and Central America, and the high-latitude ($>60°$) zones were predicted to have relatively small portions of HNO_3 associated with mineral aerosol.

Interactions of N_2O_5, O_3, and HO_2 radicals with dust were also explored and found to affect the photochemical oxidant cycle, with ozone concentrations decreasing by up to 10% in and nearby the dust source areas. The direct reaction of ozone on mineral aerosol warrants further study and could be important at mass accommodation coefficients greater than 5×10^{-5}. These dust interaction effects can be intensified on regional scales during high dust periods, where the surface areas of mineral aerosol can be an order of magnitude higher than the monthly averaged values calculated by the global model (Zhang et al. 1994).

In this paper we further explore the potential impact of mineral aerosol on tropospheric chemistry using a box model in which detailed gas-phase chemistry is combined with dust surface uptake processes. We explore the sensitivity of the dust influence to such quantities as surface reaction probabilities and the degree to which particulate nitrate is converted back into NO_x. These issues are explored under conditions representative of dust events in East Asia.

2. The combined gas-phase and dust chemistry box model

a. Simulation of properties and dynamics of mineral aerosol

Mineral aerosol has a diameter ranging from 0.1 to about 1000 μm. Large particles with a diameter greater than 40 μm usually settle out near the source regions, while the relatively small particles have a lifetime of several days and weeks and can be transported up to several thousands of kilometers. Ambient dust usually has a multilayer and multicomponent structure. The dust at and near the source regions is dry and usually has two layers: an irregularly shaped insoluble core consisting of silica and a soluble solid shell mainly consisting of carbonate and some trace metal salts (Rahn et al. 1979; Okada et al. 1990; Inoue and Yoshida 1990). Away from the sources the long-range-transported (LRT) dust usually consists of an insoluble core, a soluble solid layer, and a liquid coat composed of an aqueous solution of electrolytes (Chung and Harris 1991; Parungo et al. 1995). The composition of mineral dust is dependent on the soil composition at the source and the air constituents along the transport path. For example, dust derived from the Asian continent is enriched in SO_4^{2-}, NO_3^-, NH_4^+, Cl^-, and trace metals such as Al, Ca, Fe, Na, K, and Mg (Kang and Sang 1991; Nishikawa et al. 1991a), while the dust derived from the Sahara Desert is enriched in Ba, Ti, Mn, and Fe (Rahn et al. 1979).

The air parcels that we simulate in the box model are assumed to be far away from the dust sources and thus contain only the LRT dust particles. We assume that particles are initially dry, spherical, and charge neutral; particles have a diameter of 0.1–40 μm; and particles are internally mixed, that is, all particles at a given size have the same composition. The size distribution of LRT dust is observed to have a lognormal shape, with the largest number concentration in the accumulation mode with radii of 0.05–20 μm (Patterson and Gillette 1977; Nishikawa et al. 1991b). The number distribution can be given as

$$\frac{dN}{d\ \log r} = \frac{n}{\sqrt{2\pi}\ \log\sigma} \exp\left\{\frac{-(\log r/R)^2}{2(\log\sigma)^2}\right\}, \qquad (1)$$

where n, r, and σ are the number concentration, the number mean radius, and the standard deviation, respectively. An average density of 2.6 g cm^{-3} is used (Arao and Ishizaka 1986).

The dynamic processes involving dust simulated in the box model are nucleation, condensation, and coagulation. The dependences of these processes on particle size, temperature, relative humidity (RH), and vapor pressure of condensable species are also taken into account. The binary homogeneous nucleation of H_2SO_4 and H_2O vapor in the presence of dust is simulated based on an empirical approximation of the classic nucleation theory (Easter and Peters 1994). These fine particles can serve as nuclei for the condensable species or coagulate with one another or with dust particles to form larger particles. This mechanism is important to the formation of non-sea-salt (nss) sulfate on the surface of small dust particles. The condensation and evaporation of water vapor on the dust surface can change its size and mass. The resulting growth in the size and mass can be calculated as a function of ambient RH using an empirical formula derived from a number of aerosol measurements (Hänel 1976). In the empirical formula of Hänel (1976), the particle radius and mass are given as an explicit function of RH and mass increase coefficient, as well as densities of dry particles and pure water. Since there are no measurements on the mass increase coefficient of Asian dust, the relationships between mass increase coefficient and RH for condensation and evaporation processes are interpolated based on the measurements of maritime aerosol over the Atlantic containing Saharan dust during 16–25 April 1969 (Hänel 1976). The coagulation process is important for mineral dust in the fine size range, which may change the number and surface area of dust particles. The coagulation of particles is simulated based on the discrete form of the coagulation equation (Gelbard and Seinfeld 1980). The coagulation coefficients in the coagulation equation

are determined for size-resolved dust using the Fuchs and Sutugin (1970) formulation. These processes along with interfacial mass transfer and subsequent surface reactions are included in the box model to simulate the transformation of the microstructure and composition of particles. As a consequence, the dry particles emitted from the sources become wetted and aged as the air parcels move forward. The aged dust contains water, sulfate, nitrate, and dissolved oxidants in the coating layer. However, the chemical composition of dust is different from one size to another because all these processes are size dependent.

b. Combined gas-phase and dust chemistry

1) GAS-PHASE CHEMISTRY

The gas-phase chemistry of the box model is mainly constructed from the STEM-II regional-scale transport/chemistry/removal model (Carmichael et al. 1991). It consists of 86 chemical species and 185 gas-phase reactions. The mechanism is based on that of Lurmann et al. (1986) and modified to include low NO_x conditions and explicit reactions of isoprene. The reactions of organic peroxy radicals RO_2 and the major product ROOH are included. The rate coefficients for gas-phase reactions involving odd nitrogen and odd hydrogen species have been updated based on recent studies (Atkinson et al. 1989; DeMore and coauthors 1997). In addition, DMS (dimethyl sulfide) chemistry is included to estimate the contribution of the oceanic source to the sulfate formation.

2) POSSIBLE HETEROGENEOUS SURFACE REACTIONS ON DUST

Chemical analyses have shown that the observed elevated sulfate (SO_4^{2-}) and nitrate (NO_3^-) during Asian dust storms are not associated with dust at the source region (Carmichael et al. 1996), where the soils contain few calcium salts besides calcium carbonate (Inoue and Yoshida 1990). Calcium content of soils in the Asian arid regions ranges from 4% to 8% by weight (Wang and Wang 1995). The dust derived from these regions is likely to be alkaline and may act as an effective sink for acidic gases. Hirai et al. (1991) proposed that SO_4^{2-} and NO_3^- are absorbed and/or formed on the surfaces of wetted dust particles and displace the carbonates during the long-range transport processes. Analyses of precipitation sampled during dust events in Korea and Japan are consistent with this hypothesis and show that up to 75% of the carbonate is displaced by SO_4^{2-} and NO_3^- by the time the particles reach Korea and Japan (Nishikawa et al. 1991a). Herring et al. (1996) analyzed airborne measurements in the smoke plume from the 1991 Kuwaiti oil fires and found that SO_2 and NO_x can be rapidly removed by soil dust with a removal rate of 6.5% h^{-1} and 7.2% h^{-1} under a dust loading of 200 μg m^{-3}, respectively.

In this study, we explore heterogeneous reactions involving SO_2, NO_y^p (defined as $NO_3 + N_2O_5 + HNO_3$), H_xO_y (defined as $OH + HO_2 + H_2O_2$), and O_3 on dust surfaces. The nss SO_4^{2-} can be produced by several pathways, including heterogeneous oxidation of SO_2 (Okada et al. 1990; Luria and Sievering 1991), nucleation of H_2SO_4 with H_2O vapor, and condensation on the existing particles. Similarly, NO_3^- can be formed via direct scavenging of HNO_3, absorption and/or subsequent heterogeneous oxidation of nitrogen species by H_2O, and radicals on the dust surface (Lee and Schwartz 1981). As a consequence of dust perturbations, the photochemical oxidant cycle may be affected due to changes in the gas-phase concentrations. Both NO_y^p and H_xO_y play important roles in tropospheric O_3 photochemistry. A decrease in their concentrations could lower O_3 formation, as described in Zhang et al. (1994). Direct O_3 uptake on dust may also be responsible for the tropospheric O_3 decrease, as indicated by Dentener et al. (1996). The dust–gas-phase interactions discussed above are simulated in the study. The absorption of SO_2 and subsequent conversion to nss sulfate by dissolved oxidants such as H_2O_2, OH, and O_3 on n particle size modes may be parameterized by

$$SO_2 + O_x + X(i) \xrightarrow{H_2O} XSO_4(i), \qquad (2)$$

where O_x represents the dissolved oxidants such as O_3, OH, and H_2O_2; $X(i)$ represents the ith aerosol size bin for a total of n size bins ($i = 1, 2, \ldots, n$); and $XSO_4(i)$ represents the corresponding sulfate aerosol within the same size bin. The absorption of O_3 and H_xO_y on wetted dust particles is considered in a similar manner:

$$O_3 + X(i) \xrightarrow{H_2O} O_3(i)$$

and

$$H_xO_y + X(i) \xrightarrow{H_2O} H_xO_y(i). \qquad (3)$$

The heterogeneous reactions of NO_3 and N_2O_5 with H_2O on mineral aerosol to form particulate nitrate can be represented as

$$N_2O_5 + H_2O + X(i) \longrightarrow XNO_3(i) \qquad (5)$$

and

$$NO_3 + X(i) \xrightarrow{H_2O} XNO_3(i), \qquad (6)$$

where $XNO_3(i)$ represents the corresponding particulate nitrate formed on the surface of the ith size bin particle, $X(i)$. While HNO_3 can directly condense on wetted dust surface to form a nitrate, it could also react heterogeneously on carbonaceous aerosols to yield NO, NO_2, and H_2O (Rogaski et al. 1997). Hauglustaine et al. (1996) included the latter reaction of HNO_3 in a photochemical box model and found HNO_3/NO_x ratios in much better agreement with observations in the free troposphere. Lary et al. (1997) also argued that the same reaction may represent a significant renoxification mechanism, leading to O_3 loss in the lower stratosphere

and O_3 production in the upper troposphere. To account for both condensation and heterogeneous reactions of HNO_3, the following reaction pathway is assumed:

$$HNO_3 + X(i) \xrightarrow{H_2O} C_{NO_3^-} XNO_3(i) + C_{NO_x} NO_x, \quad (7)$$

where $C_{NO_3^-}$ and C_{NO_x} are yield coefficients for particulate nitrate and NO_x, respectively, with $C_{NO_3^-} + C_{NO_x} = 1$. Rogaski et al. (1997) reported that about two-thirds of the HNO_3 loss on the surface of amorphous carbon is converted to NO and NO_2 at room temperatures. The fraction of renoxification from HNO_3 loss on mineral dust is not available. Therefore, we use $C_{NO_3^-} = 1$ and $C_{NO_x} = 0$ in the base case simulations. The sensitivity of model predictions on selection of $C_{NO_3^-}$ and C_{NO_x} is evaluated by increasing C_{NO_x} up to two-thirds.

3) Surface uptake coefficient and overall heterogeneous loss rate

The overall heterogeneous loss rate of the above reactions, k_p, follows a pseudo–first order and can be given by Heikes and Thompson (1983):

$$k_{p,j} = \int_{r_1}^{r_2} k_{d,j}(r) n(r)\, dr, \quad (8)$$

where $n(r)$ (cm^{-4}) represents the number of particles per cubic centimeter air between particle radii r and $r + dr$. The parameter $k_{dj}(r)$ ($cm^3\ s^{-1}$) is the gas-to-particle diffusion rate constant of species j for a particle of radius r. It can be calculated by the Fuchs and Sutugin interpolation equation (Fuchs and Sutugin 1970)

$$k_{d,j} = \frac{4\pi r D_j V}{1 + \mathrm{Kn}[\lambda + 4(1 - \alpha)/3\alpha]}, \quad (9)$$

where D_j ($cm^2\ s^{-1}$) is the molecular diffusion coefficient of species j in the air; the variable V represents ventilation factor, which is close to 1; and Kn is the Knudson number, defined as the ratio of the effective mean free path of a gas molecule in air, λ, to the particle radius r. The variable α is the mass accommodation coefficient and represents the probability of reversible uptake of a gaseous species colliding with the condensed surface of interest. The sticking molecule may either penetrate the surface or be reflected back to the gas phase. While α represents the inflow flux, the net flux to the surface can be described by the uptake coefficient γ (also referred as the surface reaction probability), which is defined as the fraction of collisions with a particle that leads to irreversible loss of species on the condensed surfaces. The net flux can be influenced by several processes, including gas-phase diffusion, Henry's law of saturation, liquid chemistry, and surface chemistry. The variables α and γ are fundamental parameters in estimating k_d and k_p. The distinction between α and γ becomes important when desorption occurs. The term γ usually represents a lower limit to α when the various processes cannot be separated. However, there are many cases in which γ can be significantly higher than α. For instance, highly effective surface reactions on deliquescent aerosols or other liquid droplets can reduce interfacial mass transport, and consequently, reduce α (Jayne et al. 1996; Hanson 1997).

Although measurements of α and γ for various species on dust are very sparse, these values have been measured on other types of surfaces including water droplets, fly ash, sulfate, and carbon aerosols during the last several years. Table 1 summarizes recent measurements of α and γ of the eight modeled species: SO_2, NO_3, N_2O_5, HNO_3, OH, HO_2, H_2O_2, and O_3. As shown in Table 1, these coefficients strongly depend on the properties of the impinging gas, and the abundance and surface properties of the preexisting particles. For example, the measured α for SO_2 at 260–292 K on liquid water surfaces is about 0.11 (Worsnop et al. 1989), while it is 3×10^{-3} at room temperature on the surface of amorphous carbon (Rogaski et al. 1997). The values of α and γ may vary by several orders of magnitude. In general, they range from 0.01 to 1.0 for soluble species such as HNO_3, N_2O_5, OH, and HO_2, and 1.0×10^{-6} to 1.0×10^{-3} for less soluble species such as SO_2 and O_3.

In this study, we assume that absorption and heterogeneous reactions of the modeled species on dust surface are irreversible and gas-phase diffusion limited. These assumptions can be justified for most condensing species considered in this work when dust particles contain some water, which is most likely the case as observed by Hänel (1976). Ross and Noone (1991) and Matthijsen and Sedlak (1995) proposed destruction mechanisms of OH and HO_2 by catalytic redox reactions with copper or iron on aerosols and in clouds, respectively. The trace metal redox reactions are likely to occur with a rapid rate on wetted dust particles. Heterogeneous reactions of $SO_2$and HNO_3 occur through fast neutralization reactions with alkaline material such as calcium in dust particles (Okada et al. 1990; Dentener et al. 1996). In fact, the oxidation of S(IV) on wetted dust is essentially gas-phase diffusion limited for pH > 8 (Dentener et al. 1996). The compound N_2O_5 can be readily taken up by aqueous surfaces to form HNO_3, especially during the nighttime (Dentener and Crutzen 1993). Uptake of O_3 by aerosols is complicated and the mechanism is not clear. Fendel et al. (1995) proposed a surface adsorption mechanism for O_3 on carbon aerosols that yields O_2, CO, and CO_2 as final products, while Rogaski et al. (1997) also observed generation of O_2 from this reaction. These studies have shown that submicron carbon or iron particles can destroy ozone efficiently, with an uptake coefficient on the order of 10^{-4}–10^{-3}. Asian dust usually contains 4%–10% of iron by mass (Nishikawa 1991a; Zhang et al. 1993) and some organic carbon (Ohta 1991). Dentener et al. (1996) estimated that the O_3 uptake coefficient on the dust surface could be about 2×10^{-5} if the O_3 destruction is mostly determined by its reaction with iron.

TABLE 1. Measured mass accommodation coefficients, α, and uptake coefficients, γ, of species on various condensed phases under tropospheric temperatures.[a]

Species	α	T (K)	Condensed phase	γ	T (K)	Condensed phase
SO_2	0.11 ± 0.02	260–292	Liquid water	(1–500)E-6[b,c]	Room temp	Dry fly ash
	(3 ± 1)E-3	Room temp	Amorphous carbon			
NO_3	≥0.0025[d]	393	Liquid water	2E-4	273	Liquid water
N_2O_5	≥0.005[c]	293.1	Liquid water	0.039–0.012	293	$NH_3/H_2SO_4/H_2O$
				0.036 ± 0.004	282	Liquid water
HNO_3	0.071–0.167	282–293	Liquid water	0.038 ± 0.008	190–440	Amorphous carbon
	0.05 ± 0.01	297	Liquid water	(2.8 ± 0.3)E-2	Room temp	Solid powders of
	0.11 ± 0.01	283	73 wt% H_2SO_4			NaCl, NaBr, KCl
	>2.4E-3	295	97 wt% H_2SO_4			KBr, and $NaNO_3$
OH	>5E-4	298	97 wt% H_2SO_4	1.0	298	~96 wt% H_2SO_4
	>4E–3	275	Liquid water	>0.07	275	28 wt% H_2SO_4
	>0.07	275	28 wt% H_2SO_4	>0.2	298	96 wt% H_2SO_4
HO_2	>0.02	275	Liquid water	>0.07	275	28 wt% H_2SO_4
	>0.2	293	$NH_4HSO_4/LiNO_3$	[f] 0.023[f]	Room temp	NH_4Cl
	0.02	295	NaCl(s) or KCl(s)	[f] 0.013[f]	Room temp	$(NH_4)_2SO_4$
H_2O_2	0.18	273	Liquid water	7.8E-4[g]	300	H_2SO_4 aerosol
	>8E-4	298	96 wt% H_2SO_4			
O_3	>2E-3	292	Liquid water	(1–10)E-4	300	Carbon or iron
	>5.3E-4	273–292	Liquid water	(1 ± 0.5)E-3	298	Amorphous carbon

[a] All values are based on DeMore et al. (1997) and references therein except otherwise indicated.
[b] Read (1–500) E-6 as (1–500) × 10^{-6}.
[c] Judeikis et al. (1978).
[d] Thomas et al. (1993).
[e] Kirchner et al. (1990).
[f] Jech et al. (1982).
[g] Baldwin (1982).

The irreversibility of species uptake on dust is taken into account by using γ to replace α when calculating k_d and k_p. We further assume that the γ values for dust surface are similar to those for other surfaces present in the atmosphere due to lack of direct measurements for dust. In the base case study, γ is assumed to be 1.0 × 10^{-4} for less soluble species SO_2 and O_3, 0.01 for strongly volatile species HNO_3, and 0.1 for the other modeled species impinging on all size particles. To evaluate the impact of selected γ on dust perturbations, we also use two sets of γ values representative of the upper and the lower limits of measurements in the sensitivity study, as shown in Table 2. These values are generally consistent with measurements shown in Table 1.

c. Dust effects on photolytic rates

Mineral dust is known to have a strong influence on atmospheric radiative processes; however, it remains a controversial issue whether mineral dust increases or decreases the UV flux. Dickerson et al. (1997) have indicated that mineral dust absorbs much more radiation than does sulfate aerosol and that the absorbing dust may inhibit photochemical smog formation by reducing the UV flux. By contrast, D'Almeida et al. (1991) have reported that desert dust has a high single-scattering albedo, which may accelerate photochemical reactions and smog production by increasing the UV flux. It is beyond the scope of this study to attempt to quantify the radiative effect of dust. In this study, we assume that mineral dust absorbs the UV flux, although it may possibly exhibit strong scattering effects under some atmospheric conditions. To estimate the effect of dust on photolytic rates of species under various dust loadings, we obtain a crude parameterization by modifying the two-stream radiation model of Zdunkowski et al. (1982). We found that the magnitude of reduction in the photolytic rates varies with dust loading and vertical height. For example, the photolytic rate of NO_2 at 4 km decreased on 10 May by 5% and 30% in the presence of 50 and 500 μg cm^{-3} of dust, respectively, as compared to the nondust air.

TABLE 2. Uptake coefficients of species used in the box model study.

Species	Base values	Upper limit values	Lower limit values
HNO_3	0.01	0.1	0.001
NO_3	0.1	0.2	0.01
N_2O_5	0.1	0.2	0.01
OH	0.1	0.2	0.01
HO_2	0.1	0.2	0.01
H_2O_2	1.0 × 10^{-4}	2.0 × 10^{-4}	1.0 × 10^{-5}
O_3	1.0 × 10^{-4}	2.0 × 10^{-4}	1.0 × 10^{-5}
SO_2	1.0 × 10^{-4}	2.0 × 10^{-4}	1.0 × 10^{-5}

3. Simulation of Asian dust

Asia is one of the largest arid regions in the world, with a large amount of mineral dust derived from Takala Makan Desert, Gobi Desert, and loess areas at the upper stream of the Huang River. In addition to wind-blown dust, long-range transport of anthropogenic SO_2 and

TABLE 3. Initial conditions used in the box model study.

Components	Cheju[a]	Yaku[b]	PEM[c]
NO (ppb)	1.5	0.75	0.4
NO_2 (ppb)	0.5	0.25	0.1
HNO_3 (ppb)	0.2	0.1	0.05
NH_3 (ppb)	1.0	0.5	0.1
SO_2 (ppb)	5.0	2.0	1.0
DMS (ppb)	0.005	0.02	0.04
SO_4^{2-} (ppb)	0.8	0.7	0.6
O_3 (ppb)	50.0	40.0	30.0
NMHCs (ppb)	62.7	18.81	6.27
CO (ppb)	150	120	100
Dust (μg m^{-3})	0–500	0–500	0–500
Relative humidity (%)	80 and 30	80 and 30	80 and 30
Temperature (K)	283 and 298	283 and 298	283 and 298
UV radiation	Diurnal	Diurnal	Diurnal
Uptake coefficient (γ)	See Table 2	See Table 2	See Table 2

[a] Based on the measured data at Cheju Island, Korea.
[b] Assumed values based on Cheju and PEM conditions.
[c] Based on PEM-WEST-A data for altitudes above 3 km.

NO_x emitted from the Chinese continent has a significant impact over East Asia and thus provides sufficient gaseous sulfur and nitrogen precursors to interact with dust in the region. The model described above is used to explore the interactions between Asian dust and the gas-phase species as air parcels are transported off the continent in the mid- to lower troposphere. We assume that dust and air with specific compositions are mixed together inside a well-mixed parcel, and the parcel is then transported as a closed system. As a net result of dust emission and settling, particles persist at a certain loading level in the parcel and provide surfaces interacting with gaseous species.

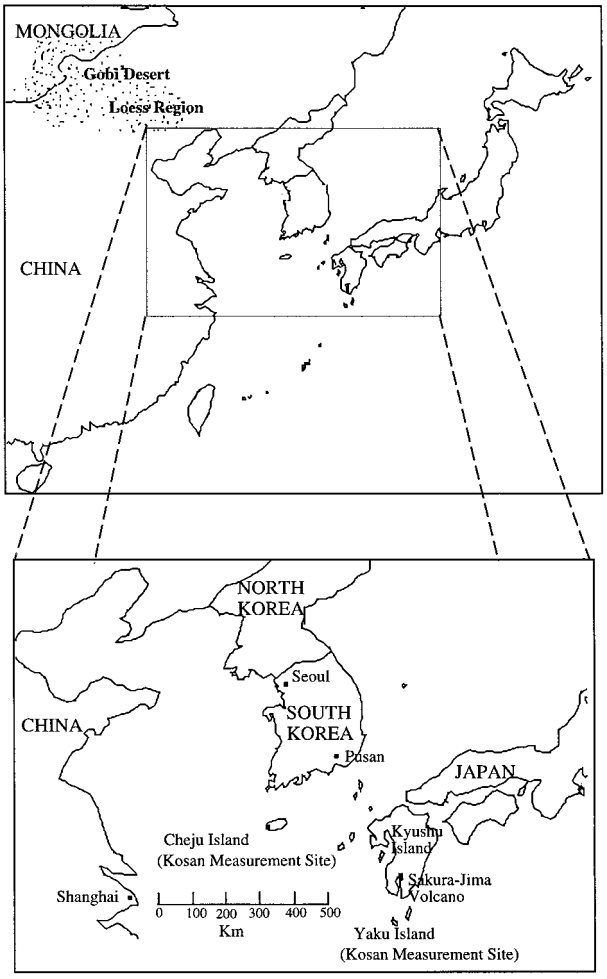

FIG. 1. Map of simulated location in East Asia.

a. Initial conditions

Three initial conditions are selected based on recent observations in East Asia as shown in Table 3. The PEM (Pacific Exploratory Mission) case is based on measurements taken over the western Pacific during the NASA PEM-WEST-A experiment (Akimoto et al. 1993). These values are typical of those found in the midtroposphere air masses that have passed over continental Asia during the previous 24 h and transported out into the Pacific Ocean. The Cheju case is based on measurements taken at Cheju Island, Korea (Hong 1993), as shown in Fig. 1. The Cheju initial conditions, selected based on the observed values for May 1992, have a much higher NO_x mixing ratio and nonmethane hydrocarbons (NMHCs) to NO_x ratio than the PEM case, reflecting the fact that air masses in this region are under the influence of the major sources in eastern China, Korea, and Japan. The Yaku case is in between the Cheju and PEM cases. Yaku Island is located in southwest Japan and about 400 km east and 200 km south of Cheju.

The simulation period is 2 days and begins at 0800 local standard time (LST) for all conditions. This timescale reflects typical transport times from China to Japan. Ambient conditions are set to be representative of those present during springtime dust storms. In the base case study, the simulated parcel is assumed to stay at a height of 4 km with a temperature of 283 K and an RH of 80%. The dust loading in the parcel is assumed to be in the range of 100–500 μg m^{-3} during the dust storms and 0–10 μg m^{-3} during non–dust storm periods. These values are selected from observations taken at Happo, Japan, during dust storms in April and May (NIES 1989), where the RH and temperature are found to be 30%–95% and 273–298 K. All simulations were performed with diurnal variation in the solar actinic flux.

b. Results and discussions

1) CHARACTERISTIC DISTRIBUTIONS AND UPTAKE RATE CONSTANTS OF ASIAN DUST

Dust observed in many sites over Japan has an extremely similar single-mode lognormal distribution. The mean radius and the standard deviation of these distributions are in the range of 0.5–0.88 μm and 1.7–1.8

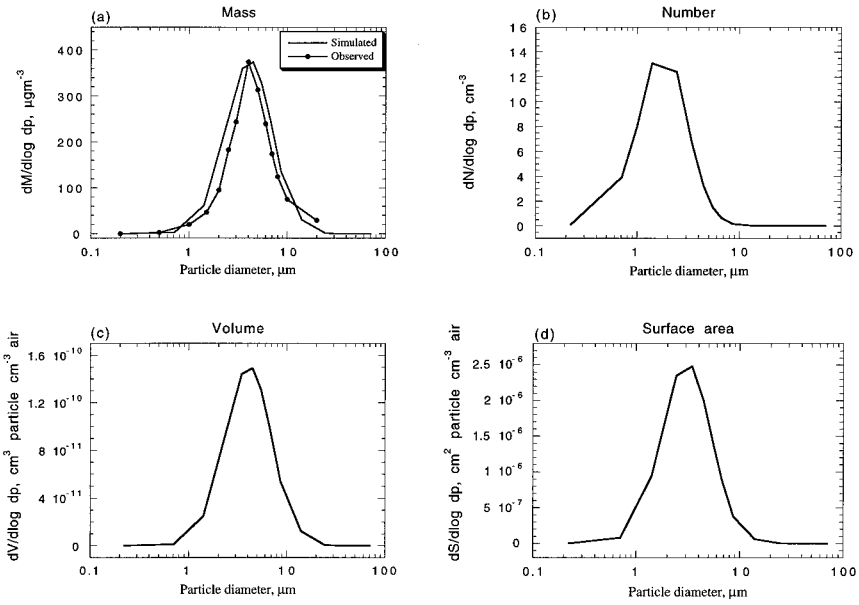

FIG. 2. The size distributions of (a) mass, (b) number, (c) volume, and (d) surface area of Asian dust.

(Arao and Ishizaka 1986; Nishikawa et al. 1991b), respectively. In this work, we take the observed size distribution in Yaku, Japan, during a dust storm of 18–20 April 1988 as an average distribution of Asian dust (total mass = 220 μg m^{-3}, r_i = 0.88 μm, and σ_i = 1.7) (Nishikawa et al. 1991b). Figure 2a shows a comparison of the simulated and the measured mass distributions in Yaku Island. Figures 2b–d show the corresponding lognormal number, volume, and surface distributions at this location. The predicted total dust number concentration, surface area, and volume in Yaku are 8.8 cm^{-3}, 1.5 cm^2 m^{-3} (air), and 8.8 $\times$ 10^{-11} cm^3 (particles) cm^{-3} (air), respectively. However, the surface area of dust available for chemical interactions during a severe dust storm (with a mass loading of 500–2000 μg m^{-3}) ranges from 5 to 21 cm^2 m^{-3} (air). The contact time for the trace gases and the dust surface is on the order of several days. Such a long timescale coupled with a large surface area makes significant interaction possible between dust and trace gas species.

The diffusion rate constant k_d and the overall heterogeneous loss rate constant k_p are important factors in determining the magnitude of heterogeneous surface uptake. Figures 3a,b show the size dependence of k_d and k_p, respectively, using base case γ values for the eight modeled species shown in Table 2. For all species, k_d increases as the particle size increases. The values of k_d are on the order of 10^{-7}–10^{-3} cm^3 s^{-1} for soluble species and the order of 10^{-9}–10^{-5} cm^3 s^{-1} for less soluble species. The values of k_p are determined by the combined effects of k_d and the number concentration. As a result of these combined effects, the maximum and minimum k_p values occur for particles with a mean diameter of 4.0 and 37.5 μm, respectively. The distribution of k_p reflects the nature of the lognormal distribution of particle number concentration.

2) THE ROLE OF DUST IN TROPOSPHERIC CHEMISTRY

(i) Dust effects on particulate nitrate and sulfate formations

Particulate NO_3^- and SO_4^{2-} formations on the dust surface are a strong function of time, surface area (varied with dust loading), and ambient precursor levels. Results from 2-day simulations show that 0.9–2.1 μg m^{-3} of NO_3^- and 0.3–10.0 μg m^{-3} of SO_4^{2-} can be formed on dust at dust loadings of 10–500 μg m^{-3} under the model conditions. The model predictions are generally consistent with measurements in the region. Nishikawa et al. (1991a) observed NO_3^- and SO_4^{2-} concentrations in Yaku Island during a typical dust storm (with a dust loading of 100–400 μg m^{-3}) are 1.2–3.8 and 6.3–16.7 μg m^{-3}, respectively. Carmichael et al. (1996) measured annual-average NO_3^- and nss SO_4^{2-} concentrations of 0.9 and 6.7 μg m^{-3}, and the spring average (March–May) of 1.5 and 7.5 μg m^{-3}, respectively, in Cheju during the period of March 1992–March 1993.

Figure 4 shows NO_3^- and SO_4^{2-} concentrations at various dust loading throughout a 2-day period under the Cheju conditions. The daytime conditions correspond to hours 0–10 (0800–1800 LST day 1) and 24–34 (0800–1800 LST day 2). As shown in Fig. 4a, NO_3^- formation increases substantially when dust loading increases from the background level (10 μg m^{-3}) to a typical value in dust storms (100 μg m^{-3}). When the dust loading further increases from 100 to 500 μg m^{-3},

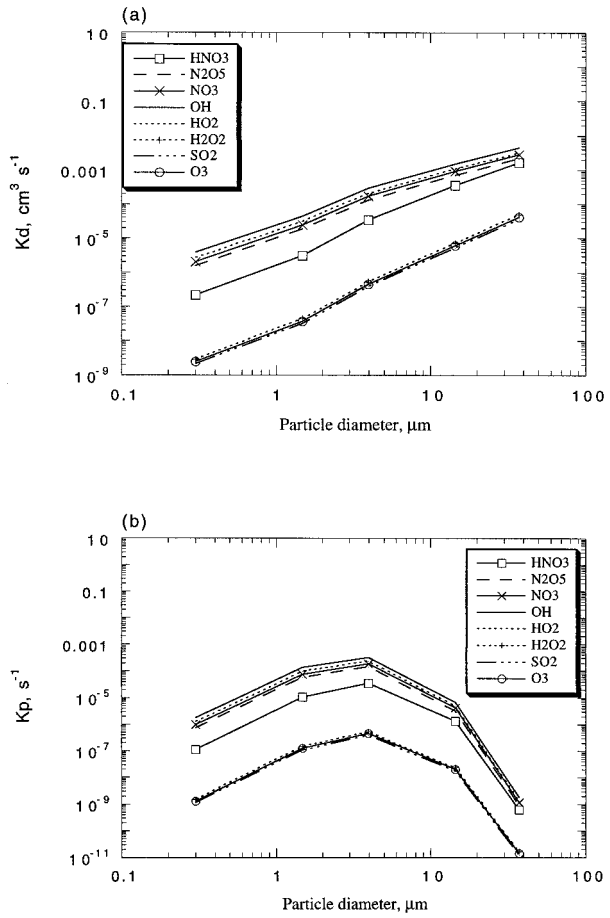

FIG. 3. (a) The diffusion rates of modeled species as a function of particle size at a dust loading of 100 μg m^{-3} and (b) overall heterogeneous loss rate of modeled species as a function of particle size at a dust loading of 100 μg m^{-3}.

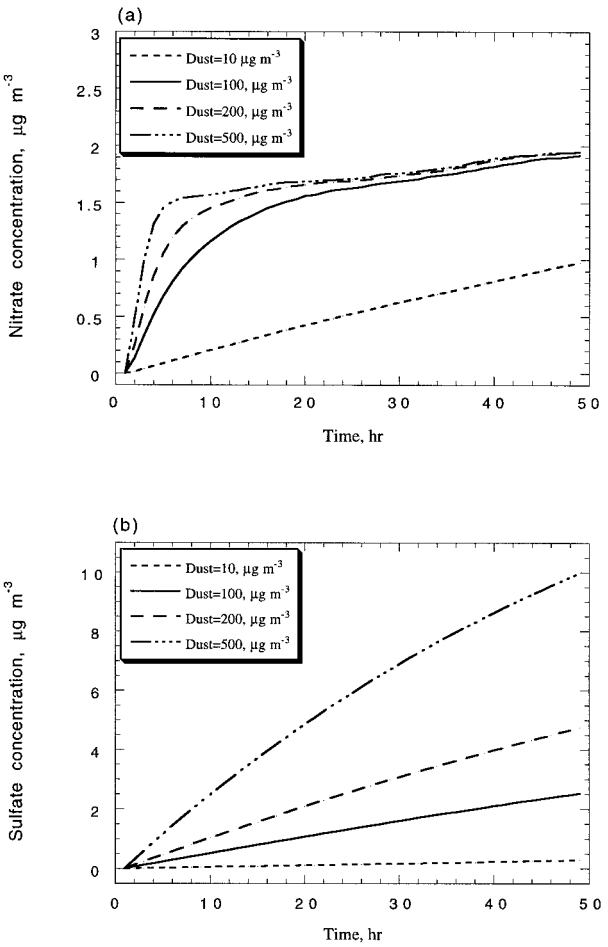

FIG. 4. Formation of (a) particulate nitrate and (b) particulate sulfate on the surface of dust at various dust loadings under Cheju base conditions.

NO_3^- formation increases rapidly during the first 20 h, but exhibits a slow increase during the remaining time, with a final yield of NO_3^- only slightly higher than that at a dust loading of 100 μg m^{-3}. This is because the nitrate formation is determined by the dust surface area and the ambient precursor concentrations. Dust loading influences both factors. Under a relatively low dust loading, NO_3^- formed on dust is always proportional to the surface area available for the reaction. When the dust loading is larger than a certain level (e.g., 100 μg m^{-3}), NO_3^- formation is initially dominated by the surface area present. However, as the gas-phase concentrations of HNO_3, NO_3, and N_2O_5 decrease, the driving force for nitrate production is limited by gas-phase diffusion to the dust surface. A different situation is found for SO_4^{2-} formation as shown in Fig. 4b. The effects of surface area always dominate since sufficient SO_2 is available for the surface uptake, which causes a persistent increase in SO_4^{2-} formation when dust loading increases from 10 to 500 μg m^{-3}.

In addition to the surface area and the ambient precursor levels, NO_3^- and SO_4^{2-} formations also strongly depend on particle size. Figures 5a,b show the lognormal mass distributions for the three cases at a dust loading of 100 μg m^{-3}. Under model conditions, most NO_3^- and SO_4^{2-} is formed on the dust surface in the size range of 1.5–10.0 μm. Their formations on dust with diameter smaller than 0.5 μm and greater than 20 μm are negligible. This is because the formations of NO_3^- and SO_4^{2-} are mainly determined by the overall heterogeneous loss rate constant, which peaks within the size range of 1.5–10.0 μm as shown in Fig. 3b. While sulfate formation is proportional to the initial SO_2 concentrations, that is, higher SO_2 yields higher sulfate, the nitrate formed on dust is limited by the available NO_y^p in the gas phase. For example, the Cheju case has the highest initial NO_x, but NO_3^- in Cheju is actually less than that in Yaku because the initial concentrations of NMHCs and oxidants in Cheju are much higher, resulting in a rapid photochemical oxidation of NO_x to produce other reactive nitrogen species such as PAN (peroxyacyl nitrate) and less NO_y^p available for dust surface uptake.

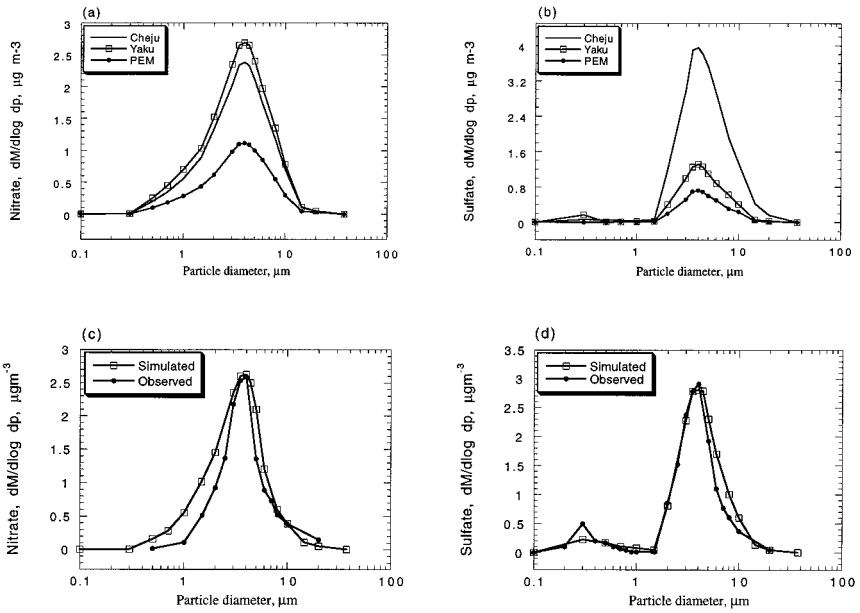

FIG. 5. The lognormal mass distribution of (a) particulate nitrate and (b) nss sulfate under model base conditions at a dust loading of 100 μg m^{-3}. The predicted and the observed mass distributions of (c) particulate nitrate and (d) nss sulfate at a dust loading of 220 μg m^{-3} at Yaku, Japan.

The predicted mass distributions of NO_3^- and SO_4^{2-} at a dust loading of 220 μg m^{-3} under Yaku conditions are plotted to compare to the measurements of Nishikawa et al. (1991a) in Figs. 5c,d, respectively. Our model predictions are consistent with observations at this location. For Yaku conditions, about 10% of the total SO_4^{2-} is found on particles with a diameter of 0.1–1.0 μm. Sulfate in the fine fraction is due mainly to nucleation of H_2SO_4 and H_2O and subsequent coagulation with fine dust particles (0.1–1.0 μm). Under conditions with a relatively low dust loading (e.g., less than 100 μg m^{-3} for the Cheju case), both surface absorption and nucleation processes are important. The SO_4^{2-} formation in the fine size range, associated with the nucleation and coagulation processes, accounts for up to 25% of the total production. As a result, the SO_4^{2-} mass exhibits a bimodal distribution. Note that the simulated sulfate in the fine size range is much lower than the observed sulfate concentrations mainly because of the use of the empirical approximation of the classic nucleation theory. At a larger dust loading (i.e., a larger surface area), the SO_4^{2-} formation due to surface uptake becomes dominant and its mass exhibits a single-mode distribution.

The predicted nss SO_4^{2-}/NO_3^- ratios under typical dust storm conditions (with a dust loading of 100–500 μg m^{-3}) after 48-h simulations are 1.3–5.1, 0.4–3.5, and 0.5–1.9 for Cheju, Yaku, and PEM cases, respectively, which are consistent with the S/N mass ratios in the anthropogenic emission in the region. For example, Akimoto et al. (1993) estimated that the S/N emission ratios from surrounding countries vary from 5, 2, and 0.6 for China, South Korea, and Japan, respectively. The ratio in the local emissions at Cheju Island is about 1–2. The mass ratios of total sulfur (nss SO_4^{2-} + SO_2) to total nitrogen (NO_3^- + NO_y) calculated from measurements obtained at Cheju in 1992 fall in the range of 1–5 (Carmichael et al. 1996).

(ii) Dust perturbation to tropospheric photochemistry

Dust can also influence the photochemical oxidant cycle in the lower and midtroposphere by changing the ambient NO_y^p and H_xO_y levels. The magnitude of dust effect is mainly determined by the uptake coefficient γ and the preexisting surface area. Figure 6a shows the changes in various species concentrations using the lower limit, the base case, and the higher limit values of γ (indicated by low, base, and high, respectively) at a dust loading of 100 μg m^{-3} after 48 h for the Cheju conditions. The dust effect (DE) is defined as the percent change in species concentrations due to dust perturbations. The DE is obtained by subtraction of results without dust from those with dust. The negative values represent a decrease in concentrations. The predicted concentration reductions range from 10.3% to 99.7% at base case conditions. The magnitude of DE varies with the prescribed γ values. For example, NO_3 concentrations decrease by 2.1%, 16%, and 24% at lower, base, and higher γ values, respectively. A rapid decrease (>90%) in HNO_3 concentrations occur at the base and high limit γ values. This is because once nitrate is produced in the gas phase, it is rapidly taken up by the dust surface, resulting in lower gaseous HNO_3 concentrations.

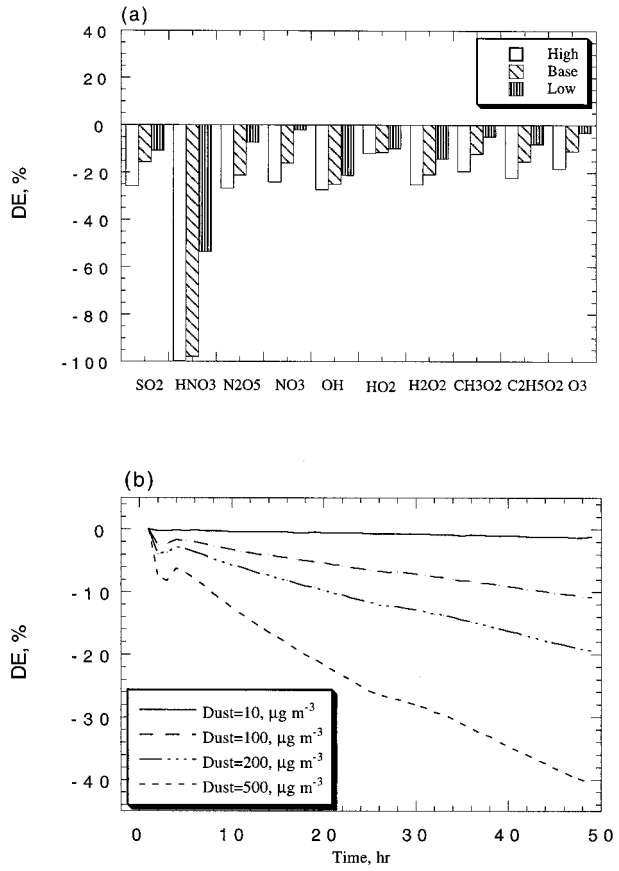

FIG. 6. (a) The effect of dust on the gas-phase concentrations expressed in terms of DE (the percent change in species concentrations due to dust perturbations) at the end of the 2-day simulation period using the upper limit (high), the base case (base), and the lower limit (low) values of uptake coefficients at a dust loading of 100 μg m^{-3} under Cheju base conditions; (b) the percent decrease in O_3 concentrations, DE, as a function of time at various dust loadings under Cheju base case conditions. The base case values of uptake coefficients used in this study are 1.0×10^{-4} for SO_2 and O_3; 0.01 for HNO_3; and 0.1 for NO_3, N_2O_5, OH, HO_2, and H_2O_2.

Coincident measurements of aerosols and ozone at a high-altitude (~2 km) surface site in Japan show that during dust storms the O_3 concentrations typically increase along with the dust concentrations. On hourly timecales, however, the O_3 and dust concentrations appear to be anticorrelated (Zhang et al. 1994). The observed decrease in O_3 ranged from 5–17 ppb for dust loading of 100–200 μg m^{-3} in East Asia. The contribution of various surface uptake processes to the local O_3 loss varies with the prescribed uptake coefficients and dust loading. Figure 6b shows the predicted percent decrease of O_3 concentrations using the base case γ values for Cheju conditions. The DE for O_3 ranges from 0.5% to 10.6%, 1.2% to 40.4%, and 2.3% to 60.5% for a dust loading of 10–500 μg m^{-3} at low, base, and high γ values, respectively. A net decrease of 2.1–21.3 ppb in O_3 concentrations was predicted for dust loading of 100–200 μg m^{-3}, which is in good agreement with the observations.

The decrease in O_3 concentration results from several pathways. For example, the direct reduction in photolytic rates leads to a decrease in O_3 formation rates. This mechanism may account for 10%–20% of total O_3 decrease under typical dust storm conditions (Zhang et al. 1994). The direct uptake of O_3 (path 3) or the destruction of important precursors (4–7) on the dust surface can also cause O_3 decrease. The relative contributions of photolytic changes (path 1), surface uptake of NO_y^p and H_xO_y (path 2), and the direct uptake of O_3 (path 3) at a dust loading of 100 and 500 μg m^{-3} under all base case conditions are summarized in Table 4. The direct uptake of O_3 (3) on dust dominates the O_3 changes (74%–87.2%) under all conditions, and the decrease in photolytic rates and the surface uptake of NO_y^p and H_xO_y (4–6) are responsible for 7.1%–20.3% and 1.4%–16.7%, respectively, depending on the initial conditions and preexisting dust loading. While the contribution of the surface uptake of NO_y^p to local O_3 loss is relatively small, these uptake processes may be more important to regional or global O_3 distribution because they significantly affect the long-range transport and the scavenging processes of NO_y^p. Since the uptake coefficient of O_3 on dust is assumed to be similar to that on carbon and iron particles measured by Fendel et al. (1995), these results are quite speculative. Our results suggest that this reaction may be an important pathway for the decrease of O_3 concentrations if the γ value is on the order of about 1×10^{-4} or greater. Further laboratory studies are needed to quantify this important parameter and to determine if this direct reaction takes place on mineral dust. The effect of dust on O_3 through the reduction of photolytic rates is also found to be important. However, this was based on a crude estimate of the effect of dust on solar actinic flux. A more detailed study is needed to quantify the dust radiative effect and the consequent impact on photolytic rates of species.

TABLE 4. The relative contributions of various pathways to the total O_3 decrease under base case conditions. The simulated pathways include the photolysis decrease (path 1), the N_xO_y uptake reactions of NO_y^p and H_xO_y (4)–(7), and the direct O_3 uptake reaction (3) (path 3).

	Dust loading = 100 μg m^{-3}				Dust loading = 500 μg m^{-3}			
Model conditions	ΔO_3 (ppb)	Path 1 (%)	Path 2 (%)	Path 3 (%)	ΔO_3 (ppb)	Path 1 (%)	Path 2 (%)	Path 3 (%)
Cheju	−7.2	20.3	1.4	78.3	−26.6	13.0	1.6	85.4
Yaku	−5.2	9.3	16.7	74.0	−18.7	11.1	9.0	79.9
PEM	−3.4	7.9	15.8	76.3	−13.6	7.1	5.7	87.2

TABLE 5. Comparison of the predicted concentrations of NO_x, HNO_3, O_3, and nitrate at the end of the 2-day simulation and the 2-day average HNO_3/NO_x ratios under nondust conditions and conditions with a dust loading of 100 μg m^{-3} and different parameterization for the heterogeneous reaction of HNO_3 on dust.

Scenarios	Species	PEM	Yaku	Cheju
No dust	NO_x (ppt)	36.9	50.0	73.3
	HNO_3 (ppt)	346.0	833.0	731.1
	O_3 (ppb)	34.7	47.1	65.9
	Nitrate (μg m^{-3})	—	—	—
	$[HNO_3/NO_x]_{avg}$	7.8	15.2	25.5
Dust = 100 μg m^{-3}	NO_x (ppt)	33.9	41.6	69.9
C_{NOx} = 0	HNO_3 (ppt)	6.6	10.9	15.3
	O_3 (ppb)	31.1	41.8	58.7
	Nitrate (μg m^{-3})	0.9	2.2	1.9
	$[HNO_3/NO_x]_{avg}$	0.8	1.2	6.5
Dust = 100 μg m^{-3}	NO_x (ppt)	46.1	60.7	83.6
C_{NOx} = ⅓	HNO_3 (ppt)	10.5	19.1	17.1
	O_3 (ppb)	32.2	43.8	60.2
	Nitrate (μg m^{-3})	0.8	1.9	1.4
	$[HNO_3/NO_x]_{avg}$	0.7	1.1	4.8
Dust = 100 μg m^{-3}	NO_x (ppt)	66.5	97.5	98.6
C_{NOx} = ⅔	HNO_3 (ppt)	18.0	39.4	22.0
	O_3 (ppb)	33.6	46.4	61.8
	Nitrate (μg m^{-3})	0.6	1.5	0.8
	$[HNO_3/NO_x]_{avg}$	0.7	1.0	3.3

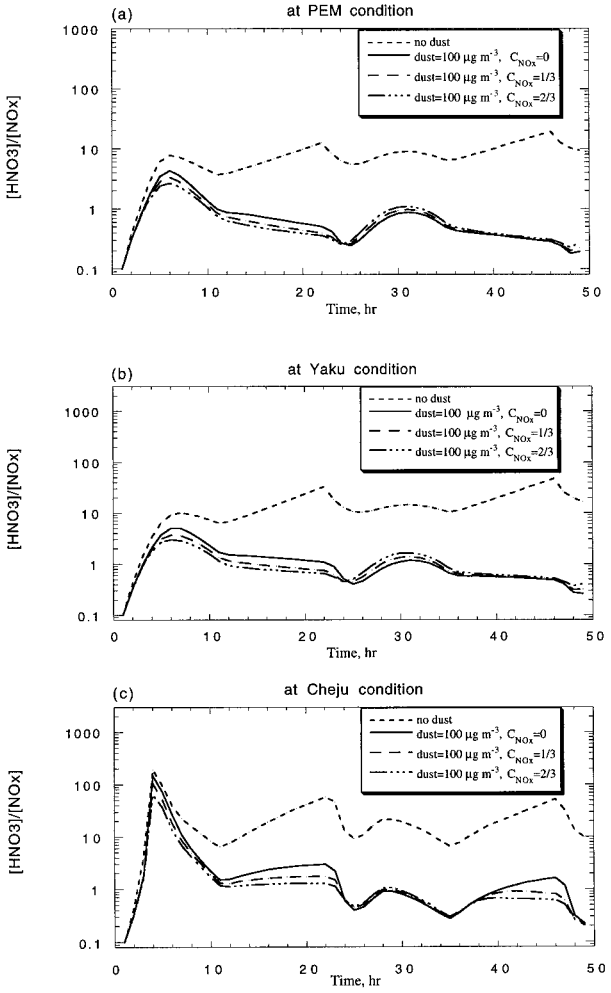

FIG. 7. The predicted HNO_3/NO_x ratios under nondust conditions and conditions with a dust loading of 100 μg m^{-3} and different parameterization for the heterogeneous reaction of HNO_3 on dust under (a) PEM, (b) Yaku, and (c) Cheju conditions.

Our base case results show that the scavenging of NO_y^p species from the gas phase to the dust surface contributes to O_3 decrease assuming no NO_x is recycled from the surface reactions. This effect, however, could be partially compensated for by renoxification from heterogeneous reaction of HNO_3 on dust surfaces (i.e., reaction 7). We evaluated the importance of renoxification by increasing the yield coefficient for NO_x, C_{NO_x}, from 0 to ⅓ and ⅔, with the corresponding yield coefficient for particulate nitrate, $C_{NO_3^-}$, of ⅔ and ⅓, respectively. The sensitivity results are summarized and compared against results from a no-dust simulation (dust loading = 0) and base case simulation (dust loading = 100 μg m^{-3}, $C_{NO_3^-}$ = ⅓ and C_{NO_x} = 0) under all conditions in Table 5. Compared to nondust conditions, the predicted NO_x concentrations are consistently lower under conditions with typical dust loading and 100% conversion of HNO_3 to nitrate (i.e., no renoxification), whereas it is always higher when HNO_3 gets converted to NO_x. The gas-phase levels of NO_x increase by 50%–100% as the recycle fraction changes from ⅓ to ⅔. The NO_x generated through this mechanism ranges from 9.2–47.5 ppt during a 2-day period. The higher NO_x levels produced by this mechanism slow down the loss in O_3 on dust, resulting in 2.5, 4.6, and 3.1 ppb of O_3 recovered under the PEM, Yaku, and Cheju conditions, respectively. These results have important implications for the chemistry of the free troposphere. Such renoxification reactions on mineral aerosol as they are transported in the midtroposphere could provide an NO_x source of 5 to 30 ppt per day, which could significantly impact the ozone budget (i.e., reduces ozone loss in the free troposphere). Similar findings were suggested by Hauglustaine et al. (1996) and Lary et al. (1997) regarding the potential importance of renoxification reactions on black carbon. The total predicted nitrate concentrations are 0.6–0.8, 1.5–1.9, and 0.8–1.4 μg m^{-3} with partial HNO_3 conversions and 0.9, 2.2, and 1.9 μg m^{-3} with 100% HNO_3 conversions under the three conditions, respectively.

The predicted HNO_3/NO_x ratios are generally overestimated by a factor of 5–10 by photochemical models, as compared to measurements in the remote troposphere (Chatfield 1994; Hauglustaine et al. 1996). The mean HNO_3/NO_x ratios between 0–3 and 3–6 km over the western Pacific obtained during PEM-WEST-A are 2.0 and 1.1, respectively (Singh et al. 1996). The predicted HNO_3/NO_x ratios as a function of simulation time under nondust conditions and conditions with a dust loading of 100 μg m^{-3} and different parameterization for the heterogeneous reaction of HNO_3 on dust for the three initial conditions are plotted in Fig. 7. As compared to

nondust conditions, the predicted HNO_3/NO_x ratios decrease substantially under a dust loading of 100 μg m^{-3}, regardless of whether and how fast the renoxification occurs. As shown in Table 5, the predicted 2-day average HNO_3/NO_x ratios without heterogeneous reactions on dust range from 7.8 to 25.5 and are brought down to 0.7–6.5 under a typical dust concentration of 100 μg m^{-3} when these surface reactions are included. These results are in agreement with modeling results of heterogeneous reaction of HNO_3 on carbonaceous aerosols presented by Hauglustaine et al. (1996) and Lary et al. (1997).

Sensitivity of the predicted O_3 levels to changes in temperature and RH was also evaluated by increasing temperature from 283 to 298 K and decreasing RH from 80% to 30%, which are typical ranges of temperature and RH observed during dust storms. In general, the higher temperature decreased slightly the effect of dust on O_3, whereas the lower RH dramatically reduced the dust effect on O_3 due to a smaller particle radius and thus lowered loss rates of O_3 and its precursors on dust.

4. Conclusions

Dust is found to have a significant influence on tropospheric trace gases and the total oxidation capacity by serving as a surface sink for gaseous species and providing reaction sites for heterogeneous oxidation of absorbed species. The presence of dust could result in a decrease in concentrations of SO_2, NO_y^p, H_xO_y, and O_3 through heterogeneous surface reactions by 10.3%–52.5%, 16.0%–99.7%, 11.3%–59.4%, and 10.9%–40.4%, respectively, under typical dust storm conditions. The decrease in solar actinic flux and the surface uptake of O_3 and its precursors were found to be important to the total O_3 decrease. For the conditions simulated, 0.9–2.1 μg m^{-3} and 0.3–10.0 μg m^{-3} of nitrate and sulfate, respectively, were formed on dust. These results are consistent with the measured values in East Asia. Size, surface area, and mass concentration of dust were shown to be important parameters, with particles in the size range of 1.5–10.0 μm contributing most significantly to their formations.

The proposed heterogeneous processes provide a plausible interpretation for the observed high nitrate and sulfate levels associated with dust and the negative correlations between dust and ozone in East Asia. This mechanism has been incorporated into our 3D model to further study the role of dust in tropospheric chemistry, with particular emphasis on the dust effects on regional and global distribution of tropospheric ozone, nitrate, and sulfate formation. The results from 3D simulations indicate that these interactions may be important in many regions of the troposphere (Zhang et al. 1996; Dentener et al. 1996; Xiao et al. 1997). Modeling results excluding heterogeneous reactions on dust tend to overpredict SO_2 and underpredict sulfate as compared to measurements in the Pacific rim region (Xiao et al. 1997).

Our results also show that the dust perturbation to gas-phase chemistry strongly depends on the preexisting dust surface, ambient conditions (i.e., gas-phase concentrations and temperature) and the selection of parameters of aerosol reactions (i.e., uptake coefficients of condensing species and yield coefficients of products). While the predicted dust effect can be accelerated by higher dust loading (i.e., higher surface areas), uptake coefficients, and relative humidities, it can also be partially compensated for by the higher NO_x levels generated through the reaction of HNO_3 on dust. If the renoxification does occur, it provides an additional source for NO_x and brings the model-predicted HNO_3/NO_x ratios closer to the measurements.

These model calculations, while valuable in identifying the potential role of heterogeneous reactions on mineral aerosol, remain highly uncertain mainly because these surfaces have not been studied from a reaction surface standpoint and basic information on many processes such as adsorption, absorption, and subsequent reactions on or in the condensed surfaces are not known. More field and laboratory research are urgently needed to better quantify the atmospheric chemical constituents, uptake coefficients, and fates of chemical species adsorbed or absorbed on the surface of mineral dust.

Acknowledgments. We wish to acknowledge the three anonymous reviewers for their useful comments on the present paper. This work was supported in part by NASA Grant NAGW-2428.

REFERENCES

Akimoto, H., D. Davis, S. Liu, and PEM-West Science Team, 1993: Atmospheric chemistry over the east Asian–northwest Pacific region. *Proc. Int. Conf. on Regional Environment and Climate Changes in East Asia,* Taipei, Taiwan, Global Change Center, National Taiwan University, 1–4.

Arao, K., and Y. Ishizaka, 1986: Volume and mass of yellow sand dust from atmospheric turbidity. *J. Meteor. Soc. Japan,* **64,** 79–93.

Atkinson, R., D. L. Baulch, R. A. Cox, R. F. Hampson, J. A. Kerr, and J. Troe, 1989: Evaluated kinetic and photochemical data for atmospheric chemistry: Supplement III. *Int. J. Chem. Kinet.,* **21,** 115–150.

Baldwin, A. C., 1982: Reactions of gases on prototype aerosol particle surfaces. *Heterogeneous Atmospheric Chemistry, Geophys. Monogr.,* No. 26, Amer. Geophys. Union, 99–102.

Carmichael, G. R., L. K. Peters, and R. D. Saylor, 1991: The Stem-II regional scale acid deposition and photochemical oxidation model. Part I. An overview of model development and applications. *Atmos. Environ.,* **25A,** 2077–2090.

——, Y. Zhang, L.-L. Chen, M.-S. Hong, and H. Ueda, 1996: Seasonal variation of aerosol composition at Cheju Island, Korea. *Atmos. Environ.,* **30,** 2407–2416.

Chatfield, R. B., 1994: Anomalous HNO_3/NO_x ratio of remote tropospheric air: Conversion of nitric acid to formic acid and NO_x. *Geophys. Res. Lett.,* **21** (24), 2705–2708.

Chung, Y.-S., and J. M. Harris, 1991: On the transport and deposition of yellow sand (dust storm). *Proc. Second IUAPPA Regional*

Conf. on Air Pollution, II, Seoul, Korea, Korea Air Pollution Research Association, 19–25.

D'Almeida, G. A., P. Koepke, and E. P. Shettle, 1991: *Atmospheric Aerosols: Global Climatology and Radiative Characteristics.* A. Deepak, 561 pp.

DeMore, W. B., and Coauthors, 1997: chemical kinetics and photochemical data for use in stratospheric modeling. JPL Publ. 97–4, National Aeronautics and Space Administration and Jet Propulsion Laboratory, California Institute of Technology, California, 266 pp. [Available from Jet Propulsion Laboratory, California Institute of Technology, Secondary Distribution, MS 512-110, 4800 Oak Grove Drive, Pasadena, CA 91109.]

Dentener, F. J., and P. J. Crutzen, 1993: Reaction of N_20_5 on tropospheric aerosols: Impact on the global distributions of NO_x, O_3, and OH. *J. Geophys. Res.*, **98,** 7149–7163.

——, G. R. Carmichael, Y. Zhang, J. Lelieveld, and P. J. Crutzen, 1996: The role of mineral aerosol as a reactive surface in the global troposphere. *J. Geophys. Res.*, **101** (D17), 22 869–22 889.

Dickerson, R. R., S. Kondragunta, G. Stenchikov, K. L. Civerolo, B. G. Doddridge, and B. N. Holben, 1997: The impact of aerosols on solar ultraviolet radiation and photochemical smog. *Science,* **278,** 827–830.

Easter, R. C., and L. Peters, 1994: Binary homogeneous nucleation: Temperature and relative humidity fluctuations, nonlinearity, and aspects of new particle production in the atmosphere. *J. Appl. Meteor.*, **33,** 775–784.

Fendel, W., D. Matter, H. Burtscher, and A. Schmidt-Ott, 1995: Interaction between carbon or iron aerosol particles and ozone. *Atmos. Environ.,* **29,** 967–973.

Fuchs, N. A., and A. G. Sutugin, 1970: *Highly Dispersed Aerosols.* Butterworth-Heinemann, 105 pp.

Gelbard, F., and J. H. Seinfeld, 1980: Simulation of multicomponent aerosol. *J. Colloid Interface Sci.*, **78,** 485–501.

Goudie, A. S., 1983: Dust storms in space and time. *Prog. Phys. Greg.*, **7,** 502–530.

Hänel, G., 1976: The properties of atmospheric aerosol particles as functions of the relative humidity at thermodynamic equilibrium with the surrounding moist air. *Advances in Geophysics,* Vol. 19, Academic Press, 73–188.

Hanson, D. R., 1997: Surface-specific reactions on liquids. *J. Phys. Chem.,* **101,** 4998–5001.

Hauglustaine, D. A., B. A. Ridley, S. Solomon, P. G. Hess, and S. Madronich, 1996: HNO_3/NO_x ratio in the remote troposphere during MLOPEX 2: Evidence for nitric acid reduction on carbonaceous aerosols? *Geophys. Res. Lett.,* **23,** 2609–2612.

Heikes, B. G., and A. M. Thompson, 1983: Effects of heterogeneous processes on NO_3, HONO, and HNO_3 chemistry in the troposphere. *J. Geophys. Res.*, **88,** 10 883–10 895.

Herring, J. A., R. J. Ferek, and P. V. Hobbs, 1996: Heterogeneous chemistry in the smoke plume from the 1991 Kuwait oil fires. *J. Geophys. Res.,* **101,** 14 451–14 463.

Hirai, E., M. Miyazaki, T. Chohji, M. Lee, M. Kitamura, and K. Yamaguchi, 1991: Effect of Kosa aerosol on inorganic components in rainwater collected from Circum–Pan–Japan–Sea area. *Proc. Second IUAPPA Regional Conf. on Air Pollution* II, Seoul, Korea, Korea Air Pollution Research Association, 27–34.

Hong, M. S., 1993: The long-range transport of air pollutants in the Pacific rim region around South Korea. Tech. Report to Korean Science Foundation, Ajou University, Suwon, Korea. [Available from Environmental Science and Engineering Research Institute, Ajou University, Suwon, Korea.]

Inoue, K., and M. Yoshida, 1990: Reports of Man-Environment System. Rep. G028-N11-01, supported by Grants in Aid for Scientific Research of Ministry of Education, Culture and Science, Japan, 97–112. [Available from Scientific Research of Ministry of Education, Culture and Science, Tsukuba, Japan.]

Jayne, J. T., D. R. Worsnop, C. E. Kolb, E. Swartz, and P. Davidovits, 1996: Uptake of gas-phase formaldehyde by aqueous acid surfaces. *J. Phys. Chem.,* **100,** 8015–8022.

Jech, D. D., P. G. Easley, and B. B. Krieger, 1982: Kinetics of reactions between free radicals and surface (aerosols) applicable to atmospheric chemistry. *Heterogeneous Atmospheric Chemistry, Geophys. Monogr.*, No. 26, Amer. Geophys. Union, 107–121.

Judeikis, H. S., T. B. Stewart, and A. G. Wren, 1978: Laboratory studies of heterogeneous reactions of SO_2. *Atmos. Environ.,* **12,** 1633–1641.

Kang, K. H., and S. E. Sang, 1991: Influence of yellow sand on TSP in Seoul. *Proc. Second IUAPPA Regional Conf. on Air Pollution* II, Seoul, Korea, Korea Air Pollution Research Association, 1–7.

Kirchner, W., F. Welter, A. Bongartz, J. Kames, S. Schweighoeffer, and U. Schurath, 1990: Trace gas exchange at the air/water interface: Measurements of mass accommodation coefficients. *J. Atmos. Chem.,* **10,** 427–449.

Lary, D. J., A. M. Lee, R. Toumi, M. J. Newchurch, M. Pirre, and J. B. Renard, 1997: Carbon aerosols and atmospheric photochemistry. *J. Geophys. Res.*, **102,** 3671–3682.

Lee, Y. N., and S. E. Schwartz, 1981: Evaluation of the rate of uptake of nitrogen dioxide by atmospheric and surface liquid water. *J. Geophys. Res.*, **86,** 11 971–11 983.

Luria, M., and H. Sievering, 1991: Heterogeneous and homogeneous oxidation of SO_2 in the remote marine atmosphere. *Atmos. Environ.,* **25A,** 1489–1496.

Lurmann, F., A. Lloyd, and A. Atkinson, 1986: A chemical mechanism for use in long-range transport/acid deposition computer modeling, *J. Geophys. Res.,* **91,** 10 905–10 936.

Matthijsen, J., and D. L. Sedlak, 1995: Cloud model experiments of the effect of iron and copper on tropospheric ozone under marine and continental conditions. *Meteor. Atmos. Phys.*, **57,** 43–60.

NIES, 1989: Studies on the methods for long-term monitoring of environmental pollutants in the background regions and atmospheric pollutants on the remote island and mountains: Concentrations and variations. Res. Rep. R-123, National Institute for Environmental Studies, Tsukuba, Japan, 146–164 pp. [Available from National Institute for Environmental Studies, Japan Environment Agency, P.O. 16-2 Onogawa, Tsukuba, Ibaraki, 305 Japan.]

Nishikawa, M., S. Kanamori, N. Kanamori, and T. Mizoguchi, 1991a: Kosa aerosol as eolian carrier of anthropogenic material. *Sci. Total Environ.,* **107,** 13–27.

——, ——, ——, and ——, 1991b: Ion equivalent balance in water soluble constituents of Kosa aerosol (in Japanese). *J. Aerosol Res.,* Japan **6,** 157–164.

Ohta, K., 1991: Aerosol chemical composition of Kosa. *Kosa,* K. Higuchi, Ed., Kokon-shoin Publishers.

Okada, K., H. Narus, T. Tanaka, and O. Nemoto, 1990: X-ray spectrometry of individual Asian dust-storm particles over the Japanese islands and the North Pacific Ocean. *Atmos. Environ.,* **24A,** 1369–1378.

Oltmans, S. J., and H. Levy II, 1992: Seasonal cycle of surface ozone over the western North Atlantic. *Nature,* **358,** 11 174–11 180.

Parungo, F., and Coauthors, 1995: Asian dust storms and their effects on radiation and climate. STC Rep. 2906. [Available from Science and Technology Corporation, 101 Research Drive, Hampton, VA 23666.]

Patterson, E. M., and D. A. Gillette, 1977: Commonalities in measured size distributions for aerosols having a soil-derived component. *J. Geophys. Res.,* **82,** 2074–2082.

Prospero, J. M., and D. L. Savoie, 1989: Nitrate concentrations over the Pacific: Oceanic background and continental impacts. *Nature,* **339,** 687–689.

——, R. A. Claccum, and R. T. Nees, 1981: Atmospheric transport of soil dust from Africa to South America. *Nature,* **289,** 570–572.

Pye, K., 1987: *Aeolian Dust and Dust Deposits.* Academic Press, 334 pp.

Rahn, K. A., R. D. Borys, G. E. Shaw, L. Schutz, and R. Jaenicke, 1979: Long-range impact of desert aerosol in atmospheric chemistry: Two examples. *Saharan Dust,* C. Morales, Ed., John Wiley and Sons, 243–266.

Rogaski, C. A., D. M. Golden, and L. R. Williams, 1997: Reactive uptake and hydration experiments on amorphous carbon treated with NO_2, SO_2, O_3, HNO_3, and H_2SO_4. *Geophys. Res. Lett.*, **24,** 381–384.

Ross, H. B., and K. J. Noone, 1991: A numerical investigation of the destruction of peroxy radical by Cu ion catalyzed reactions on aerosol particles. *J. Atmos. Chem.*, **12,** 121–136.

Savoie, D. L., and J. M. Prospero, 1989: Comparison of oceanic and continental sources of non-sea–salt sulfate over the Pacific Ocean. *Nature,* **339,** 685–687.

——, ——, and E. S. Saltzman, 1989: Non-seasalt sulfate and nitrate in tradewind aerosols at Barbados: Evidence for long-range transport. *J. Geophys. Res.,* **94,** 5069–5080.

Schütz, L., and R. Jaenicke, 1974: Particle number and mass distributions above 10^{-4} cm radius in sand and aerosol of the Sahara desert. *J. Appl. Meteor.,* **13,** 863–870.

Sheehy, D. P., 1992: A perspective on desertification of grazing land ecosystems in North China. *Ambio,* **21,** 303–307.

Singh, H. B. and Coauthors, 1996: Reactive nitrogen and ozone over the western Pacific: Distribution, partitioning, and sources. *J. Geophys. Res.,* **101,** 1793–1808.

Tegen, I., and I. Fung, 1994: Modeling of mineral dust in the atmosphere: Sources, transport, and optical thickness. *J. Geophys. Res.,* **99,** 22 897–22 914.

Thomas, K., A. Volz-Thomas, and D. Kley, 1993: On the interaction of NO_3 radicals with aqueous solution: Estimation of the Henry coefficient and the mass accommodation coefficient (in German). Forschungszentrum Juelich GmbH, Inst. Fuer Chemie 2—Chemie der Belasteten Atmosphaere, Wuppertal Univ. [NTIS DE94739080.]

Wang, W., and T. Wang, 1995: On the origin and the trend of acid precipitation in China. *Water, Air, Soil Pollut.,* **85,** 2295–2300.

Worsnop, D. R., M. S. Zahniser, C. E. Kolb, J. A. Gardner, L. R. Watson, J. M. Van Doren, J. T. Jayne, and P. Davidovits, 1989: Temperature dependence of mass accommodation of SO_2 and H_2O_2 on aqueous surfaces. *J. Phys. Chem.,* **93,** 1159–1172.

Xiao, H., G. R. Carmichael, J. Durchenwald, D. Thornton, and A. Bandy, 1997: Long-range transport of SO_x and dust in East Asia during the PEM-B experiment. *J. Geophys. Res.*, **102** (D23), 28 589–28 612.

Zdunkowski, W., W. Panhans, R. Welch, and G. Korb, 1982: Radiation scheme for circulation and climate models. *Beitr. Phys. Atmos.*, **55,** 215–238.

Zhang, J., S. M. Liu, X. Lu, and W. W. Huang, 1993: Characterizing Asian wind-dust transport to the northwest Pacific Ocean: Direct measurements of the dust flux for two years. *Tellus,* **45B,** 335–345.

——, Y. Sunwoo, G. R. Carmichael, and V. R. Kotamarthi, 1994: Photochemical oxidant processes in the presence of dust: An evaluation of the impact of dust on particulate nitrate and ozone formation. *J. Appl. Meteor.,* **33,** 813–824.

——, L.-L. Chen, G. R. Carmichael, and F. Dentener, 1996: The role of mineral aerosol in tropospheric chemistry. *Air Pollution Modeling and Its Application XI,* S.-E. Gryning and F. A. Schiermeier, Eds., Plenum Press, 239–248.